Power System Technology **Volume 48 · Number 1 · 2024**
ISSN: 1000-3673

Association Analysis and Complementary Application of BTTC and EEAC Method for Rotor Angle Stability

Zheng, C., Sun, H.
Xinxiang University, Xinjiang, China

ABSTRACT
This article provided a detailed analysis and discussion on the key points that affect the calibration accuracy of binocular cameras. A planar calibration board based on solid dot marker guided matching was designed, and its superiority over traditional calibration boards through experiments were verified. At the same time, an improved camera calibration method based on two-step RANSAC algorithm was proposed. The calibration flow of binocular camera was designed for the improved calibration method. This method solves the problem of difficult target size calibration in images, while it has broad application prospects in the fields of online measurement of image targets and small target image recognition.

1. INTRODUCTION

In recent years, the rapid development of computer vision has gradually been applied in fields such as industrial automation, agricultural product picking, national defense aerospace, biomedicine, etc. Visual measurement has a wide range of application prospects. Many domestic and foreign enterprises, universities and scholars have conducted in-depth research in the field of visual measurement. Many of them achieved good research results in theoretical innovation and practical application [1].

Foreign vision measurement technology develops rapidly. In the early 1980s, American scientist Marr et al. proposed the theoretical framework of Marr vision for the first time, which promoted the development of computer vision. At the same time, developed countries mainly in the United States began to develop a variety of vision-based detection systems for different fields of detection. Many foreign companies are committed to the research of visual measurement technology, such as the United States OGP company, the United States NI company, Germany Leica company, etc. Most of these companies have a long history and have outstanding representative works in the field of visual measurement. They developed visual measurement systems, such as OGP's SmartScope 3D optical measurement system, which is a set of intelligent geometric quantity measurement systems with multiple sensors [2]. According to the shape, size, surface color, roughness and other information of the workpiece, different measurement sensors can be selected, and a variety of measurement schemes can be formulated to accurately detect the geometric size of the part, which is especially suitable for multi-dimensional measurement of complex parts [3-5].

Computer vision measurement methods have wide applications and can generally be divided into two categories: active measurement and passive measurement. Active measurement includes linear structured light, surface structured light, TOF technology, etc. [6-7]. Passive measurement includes monocular measurement, binocular measurement, etc.

As a representative of active measurement, structured light plays an important role in 3D reconstruction such as cultural relic reconstruction, facial recognition, reverse engineering and so on.

2. THE PRINCIPLE OF THREE-DIMENSIONAL MEASUREMENT FOR BINOCULAR VISION

Binocular vision utilizes the principle of triangular similarity to locate three-dimensional coordinates of any point in space. For the calibrated binocular measurement system, the only thing to do is to find the image coordinates of the target points on the left and right camera imaging surface. then the three-dimensional coordinates of the target points through the transformation relationship of the coordinate system is obtained [8].

This section first briefly introduces the transformation relationship of commonly used coordinate system in visual measurement, which lays a foundation for the following overview of the three-dimensional measurement principle of binocular vision. Then, according to the existing two kinds of binocular measurement models, the three-dimensional measurement principles are derived from shallow to deep [9-10].

It is especially emphasized that the coordinate transformation and model derivation introduced in this section do not consider the influence of lens distortion and other factors on coordinate distortion. The camera distortion model will be summarized in Chapter 2.

2.1. The transformation relationship of common coordinate systems in visual measurement

Visual measurement by single camera imaging is mainly based on the principle of triangulation, coordinate transformation of the feature points detected on the camera imaging surface, and the absolute coordinates in the objective coordinate system are used to describe the location of the feature points, so as to achieve the purpose of positioning detection. Visual measurement is based on the transformation of various coordinate systems. The commonly used coordinate systems and transformation relationships are as follows.

2.1.1. World coordinate system

The world coordinate system is a three-dimensional coordinate system that we define ourselves, which conforms to the right-hand coordinate system guidelines, the unit is usually mm, generally represented by O_XYZ,as shown in Fig.1(a).

2.1.2. Image coordinate system

The image coordinate system is a two-dimensional coordinate system located on the imaging surface of the camera, as shown in Fig.1(b), and is a collective term for the following two coordinate systems [11-13]. Image physical coordinate system: the unit is usually mm, generally represented by O_1_xy; Image pixel coordinate system: unit is pixel, generally represented by O_0_uv.

2.1.3. Camera coordinate system [14]

Camera coordinate system: The unit is usually mm, usually represented by $O_c\_X_cY_cZ_c$, the Z_c axis intersects the optical center O_1 of the image physical coordinate system, as shown in Fig.1(c).

2.1.4. Transformation relations between coordinate systems [15]

The transformation of world coordinates $P(X,Y,Z)$ to camera coordinates $P(X,Y,Z)$ can be described by equation (1).

$$\begin{bmatrix} X_c \\ Y_c \\ Z_c \end{bmatrix} = [R] \begin{bmatrix} X \\ Y \\ Z \end{bmatrix} + t \qquad \text{or} \qquad \begin{bmatrix} X_c \\ Y_c \\ Z_c \\ 1 \end{bmatrix} = \begin{bmatrix} R & t \\ 0 & 1 \end{bmatrix} \begin{bmatrix} X \\ Y \\ Z \\ 1 \end{bmatrix} \tag{1}$$

In the equation, $\boldsymbol{R}$ is the rotation matrix of 3×3 and t is the translation vector of 3×1.

As shown in Fig.1(c), the transformation of camera coordinates $P_c(X_c, Y_c, Z_c)$ to image physical coordinates $p(x,y)$ is as follows:

$$\begin{cases} x = f\frac{X_c}{Z_c} \\ y = f\frac{Y_c}{Z_c} \end{cases} \Rightarrow Z_c \begin{bmatrix} x \\ y \\ 1 \end{bmatrix} = \begin{bmatrix} f & 0 & 0 & 0 \\ 0 & f & 0 & 0 \\ 0 & 0 & 1 & 0 \end{bmatrix} \begin{bmatrix} X_c \\ Y_c \\ Z_c \\ 1 \end{bmatrix} \tag{2}$$

In the equation, f is the focal length of the camera, the unit is mm.

As shown in Fig. 1 (b), the transformation of image physical coordinates $p_1(x,y)$ to image pixel coordinates $p_0(u,v)$ is as follows [16-18]:

$$\begin{cases} u = \frac{x}{dx} + u_0 \\ v = \frac{y}{dy} + v_0 \end{cases} \Rightarrow \begin{bmatrix} u \\ v \\ 1 \end{bmatrix} = \begin{bmatrix} \frac{1}{dx} & 0 & u_0 \\ 0 & \frac{1}{dy} & v_0 \\ 0 & 0 & 1 \end{bmatrix} \begin{bmatrix} x \\ y \\ 1 \end{bmatrix} \tag{3}$$

In the equation, d_x and d_y are the physical dimensions of camera pixels in the horizontal and vertical directions, the unit is mm.

According to equations (1), (2) and (3), the transformation from world coordinates $P(X,Y,Z)$ to image pixel coordinates $p_0(u,v)$ is as follows [19]:

$$s \begin{bmatrix} u \\ v \\ 1 \end{bmatrix} = \begin{bmatrix} f_x & 0 & u_0 & 0 \\ 0 & f_y & v_0 & 0 \\ 0 & 0 & 1 & 0 \end{bmatrix} \begin{bmatrix} R & t \\ 0 & 1 \end{bmatrix} \begin{bmatrix} X \\ Y \\ Z \\ 1 \end{bmatrix} \tag{4}$$

In the equation, s is the scale factor; Both $[u \quad v \quad 1]$ and $[X \quad Y \quad Z \quad 1]$ are homogeneous coordinate vectors.

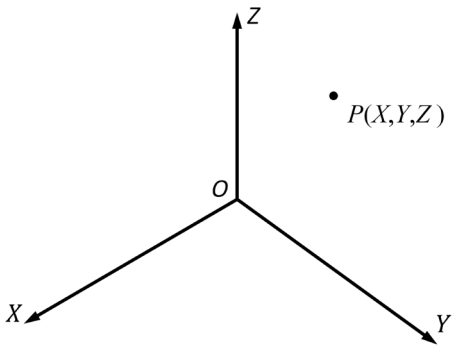

a) World coordinate system O_XYZ

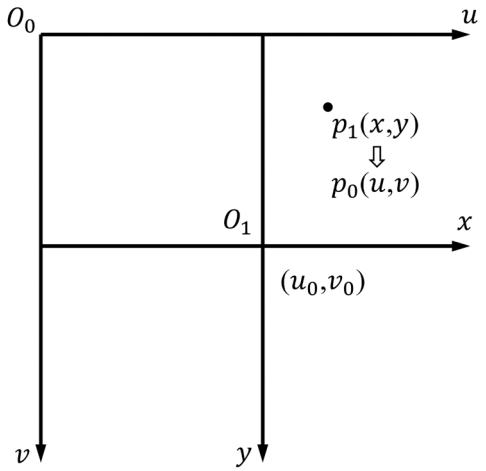

b) Image pixel coordinate system O_0_uv and image physical coordinate system O_1_xy

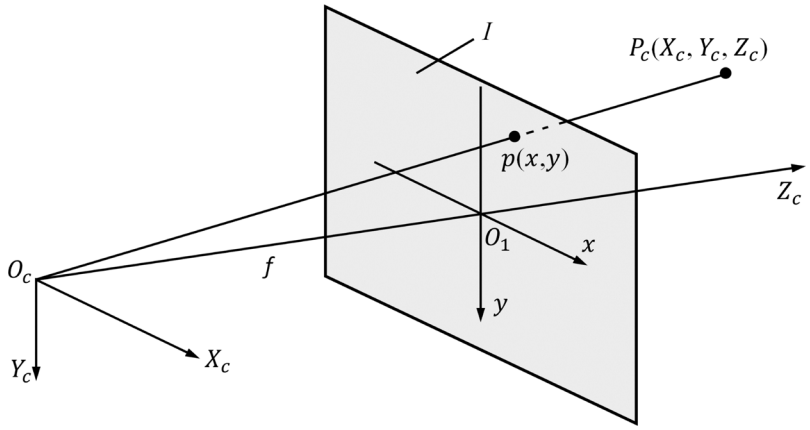

c) Camera coordinate system $O_c_X_cY_cZ_c$and Image physical coordinate system O_1_xy

Fig.1. The Transformation Relationship of Common Coordinate Systems in Visual Measurement

2.2. Standard binocular vision 3D measurement model

Fig. 2 shows the three-dimensional measurement model of standard binocular vision, which means that in an ideal scenario, assuming the focal length f of the left and right cameras is the same, the main optical axes of the two cameras are strictly parallel. The left and right image planes I_l and I_r are located in the same plane. Generally, the default world coordinate system O_XYZ coincides with the left camera coordinate system $O_{cl}\_X_lY_lZ_l$, so that the projection coordinates of space points on the left and right cameras are $p_l(x_l, y_l)$ and $p_r(x_r, y_r)$, respectively[20-21].

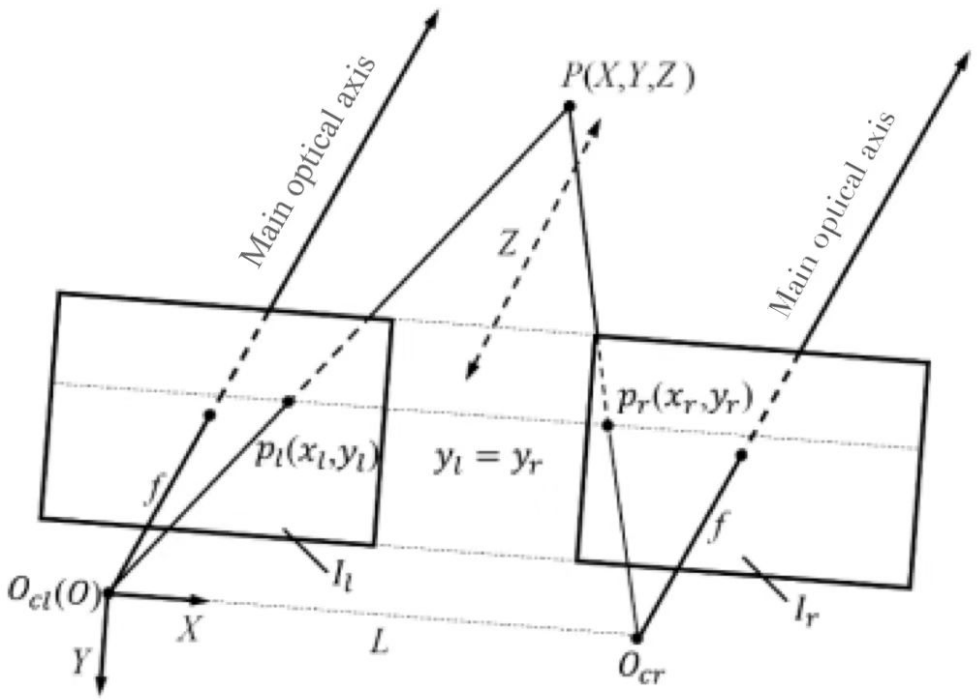

Fig. 2. Standard binocular vision 3D measurement model

Under the standard binocular vision imaging system, the vertical coordinates of the projection point p are the same, $y_l = y_r$. Based on triangular similarity, it can be concluded that [22]:

$$\begin{cases} x_l = f\frac{X}{Z} \\ x_r = f\frac{(X-L)}{Z} \\ y_l = y_r = f\frac{Y}{Z} \end{cases} \tag{5}$$

In the equation, L is referred to as the baseline.

According to equation (5), the world coordinates of point P can be obtained as [23-24]:

$$\begin{cases} X = x_l \frac{Z}{f} \\ Y = y_l \frac{Z}{f} \\ Z = \frac{fL}{x_l - x_r} \end{cases} \tag{6}$$

In the equation, $x_l - x_r$ is called parallax and is generally represented by d, that is, $d = x_l - x_r$. As can be seen from Equation (6), we only need to find the image coordinates p_l and p_r of the spatial point P in the left and right images, as well as the corresponding parallax d, to obtain the world coordinate (X, Y, Z) of point P.

2.3. General binocular vision 3D measurement model

In the actual binocular measurement system, the optical axes of the two cameras cannot be guaranteed to be absolutely parallel during installation, nor can the focal lengths f of the two cameras be completely consistent. In this case, it is impossible to ensure that the vertical coordinates of point p_l and p_r projected by space point P on the left and right cameras are consistent. This model is called the general binocular vision three-dimensional measurement model.

As shown in Fig. 3, the world coordinate of space point P is (X, Y, Z), and the coordinates of point P in the left and right camera coordinate systems are $P_{cl}(X_l Y_l Z_l)$ and $P_{cr}(X_r Y_r Z_r)$ respectively. Similarly, the projection coordinates of point P on both cameras are $p_l(x_l, y_l)$ and $p_r(x_r, y_r)$ respectively.

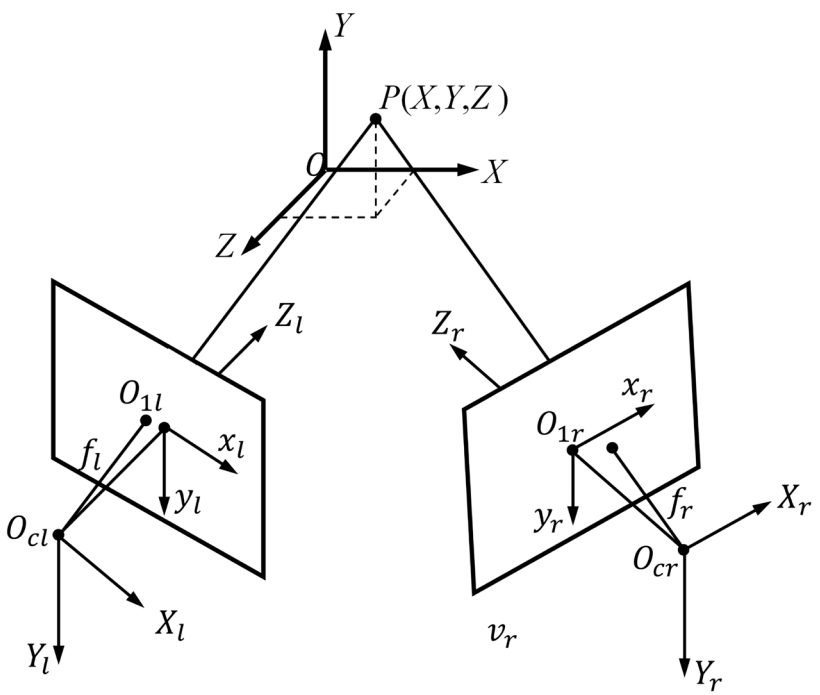

Fig. 3. General binocular vision 3D measurement model

According to spatial geometric relationships, without considering errors [25], rays $O_{cl}P$ and $O_{cr}P$ will intersect at a point P in space. Based on the triangular similarity relationship, the equations for rays $O_{cl}P$ and $O_{cr}P$ are as follows:

$$Z_l \begin{bmatrix} x_l \\ y_l \\ 1 \end{bmatrix} = \begin{bmatrix} f_l & 0 & 0 \\ 0 & f_l & 0 \\ 0 & 0 & 1 \end{bmatrix} \begin{bmatrix} X_l \\ Y_l \\ Z_l \end{bmatrix} \tag{7}$$

$$Z_r \begin{bmatrix} x_r \\ y_r \\ 1 \end{bmatrix} = \begin{bmatrix} f_r & 0 & 0 \\ 0 & f_r & 0 \\ 0 & 0 & 1 \end{bmatrix} \begin{bmatrix} X_r \\ Y_r \\ Z_r \end{bmatrix} \tag{8}$$

The transformation matrix between camera coordinate system $O_{cl}\_X_lY_lZ_l$ and $O_{cr}\_X_rY_rZ_r$ can be represented by M_{lr}, which can be obtained through binocular camera calibration, Therefore, the coordinate transformation relationship between the two camera coordinate systems is [26]:

$$\begin{bmatrix} X_r \\ Y_r \\ Z_r \end{bmatrix} = \boldsymbol{M_{lr}} \begin{bmatrix} X_l \\ Y_l \\ Z_l \\ 1 \end{bmatrix} = \begin{bmatrix} r_1 & r_2 & r_3 & t_x \\ r_4 & r_5 & r_6 & t_y \\ r_7 & r_8 & r_9 & t_z \end{bmatrix} \begin{bmatrix} X_l \\ Y_l \\ Z_l \\ 1 \end{bmatrix}, \ \boldsymbol{M_{lr}} = [\boldsymbol{R_{lr}} | \boldsymbol{t_{lr}}] \tag{9}$$

Substituting Eq. (9) into Eq. (8), the following can be obtained:

$$Z_r \begin{bmatrix} x_r \\ y_r \\ 1 \end{bmatrix} = \begin{bmatrix} f_r r_1 & f_r r_2 & f_r r_3 & f_r t_x \\ f_r r_4 & f_r r_5 & f_r r_6 & f_r t_y \\ r_7 & r_8 & r_9 & t_z \end{bmatrix} \begin{bmatrix} X_l \\ Y_l \\ Z_l \\ 1 \end{bmatrix} \tag{10}$$

By simultaneous Eq. (7) and Eq. (10), the coordinates of space point P in the left camera coordinate system can be solved as follows [27]:

$$\begin{cases} X_l = Z_l \dfrac{x_l}{f_l} \\ Y_l = Z_l \dfrac{y_l}{f_l} \\ Z_l = \dfrac{f_l(f_r t_x - x_r t_z)}{x_r(r_7 x_l + r_8 y_l + f_l r_9) - f_r(r_1 x_l + r_2 y_l + f_l r_3)} \\ \quad = \dfrac{f_l(f_r t_y - y_r t_z)}{y_r(r_7 x_l + r_8 y_l + f_l r_9) - f_r(r_4 x_l + r_5 y_l + f_l r_6)} \end{cases} \tag{11}$$

According to the calibration parameters, the focal length f_l and f_r of the two cameras, as well as the transformation matrix $\boldsymbol{M_{lr}}$. If $p_l(x_l, y_l)$ and $p_r(x_r, y_r)$ are also known, the three-dimensional coordinates of point P can be obtained according to equation (11). However, in the general binocular imaging mode, the vertical coordinates of the projection points p_l and p_r of point P are inconsistent, which increases the difficulty of matching the corresponding

points of features. It is usually that the general binocular vision measurement model into the standard binocular model through binocular calibration parameters is calibrated first. Then the detection and matching of the projection points are carried out [28-29].

3. DESIGN OF PLANE CALIBRATION BOARD BASED ON SOLID DOT MARKER GUIDE MATCHING

From the analysis in the previous section, it can be seen that the matching accuracy between the imaging points of the calibration plate on the left and right cameras directly affects the calibration accuracy of the binocular camera. Only when the calibration plate meets the two basic features mentioned above can the precise positioning and matching of the calibration plate feature points be completed. Although the planar calibration plates used by Halcon and MATLAB calibration toolbox meet the two basic characteristics of calibration plates, they have certain limitations in practice:

(1) There is perspective projection error in the center coordinates of the solid dot calibration plate in camera imaging,
(2) To perform dual target timing, the left and right cameras must capture complete calibration images.

This article improves the design of commonly used calibration boards based on their limitations and combines the advantages of solid dot calibration boards and checkerboard calibration boards to design a planar calibration board based on solid dot marker guided matching. As shown in Fig.4, the specification and size of the calibration plate is 238×182 mm, with 13×17 black and white square squares, the side length is 14 mm, and the radius of the solid dot is 5 mm. The calibration plate has the following characteristics.

(1) The calibration plate uses corner points as the calibration feature points, which satisfies feature 1 of the calibration plate. The four solid dots embedded in the middle of the checkerboard can be used as the direction markers of the calibration board to ensure that the checkerboard corner points have unique coordinate positioning, satisfying characteristic 2 of the calibration board.
(2) This calibration board combines solid dots and black and white checkerboard grids, showcasing their respective advantages: Solid dots have strong anti-interference ability and are easy to identify and detect, so they are especially suitable as mark points. The positioning accuracy of black and white checkerboard corner points is higher, it can still position with high precision after perspective projection of corner features.
(3) The four solid dot marks are located in the center of the calibration plate. When the binocular camera calibration is carried out, it is not necessary to shoot a complete calibration plate image deliberately, but to ensure that the acquired calibration image contains the four-mark points.

In order to better explain the advantages of the planar calibration board designed in this article compared to traditional calibration boards. This section describes the positioning and matching of the feature points of the calibration plate and simulates the special situation of shooting the calibration image, that is, the binocular camera has not collected the complete calibration plate, and then carries out the positioning and matching of the feature points of the calibration plate in this case.

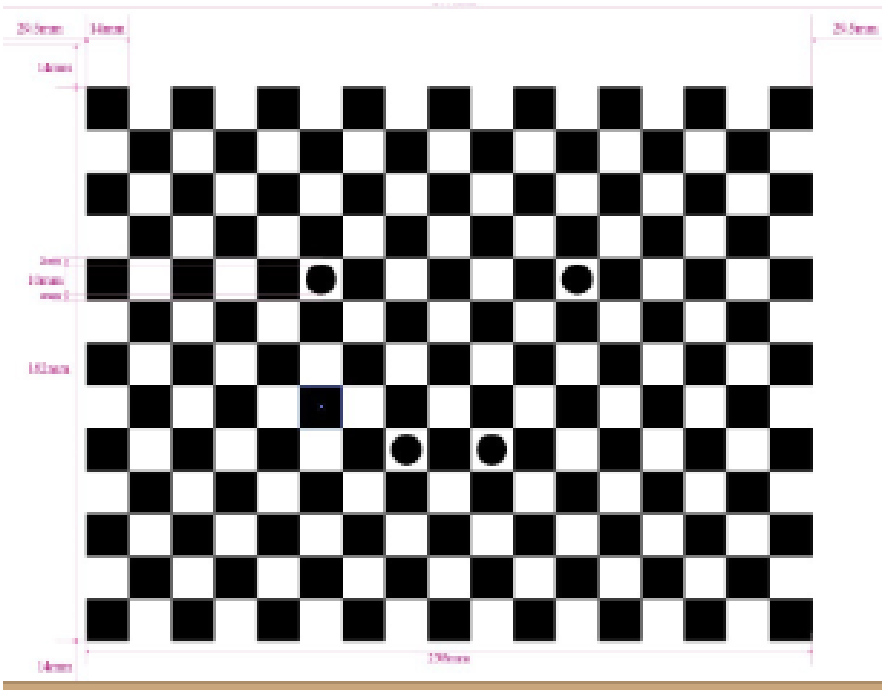

a) Design drawing

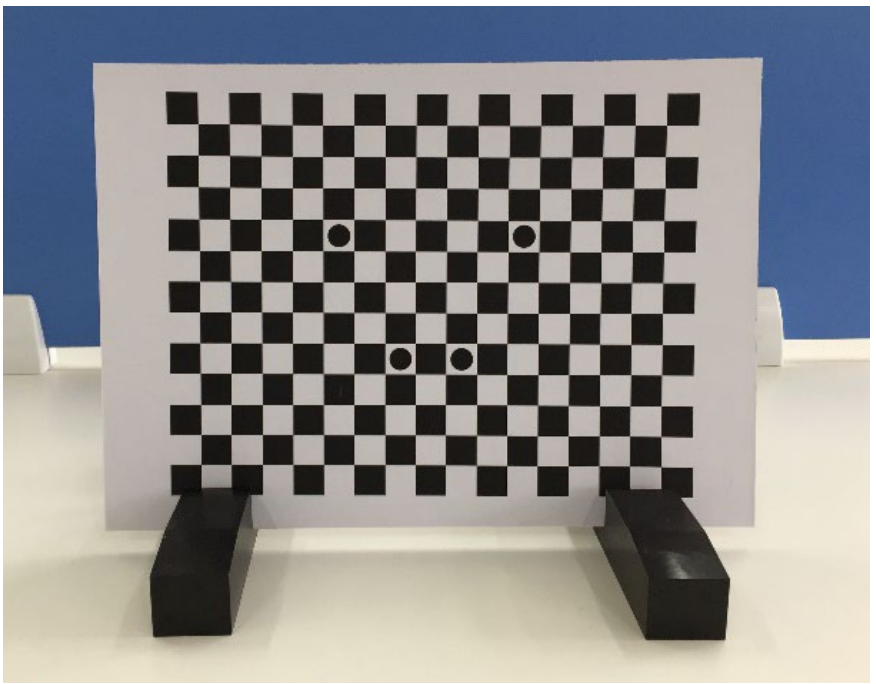

b) Physical drawing

Fig. 4. Plane calibration board based on solid dot mark guide matching.

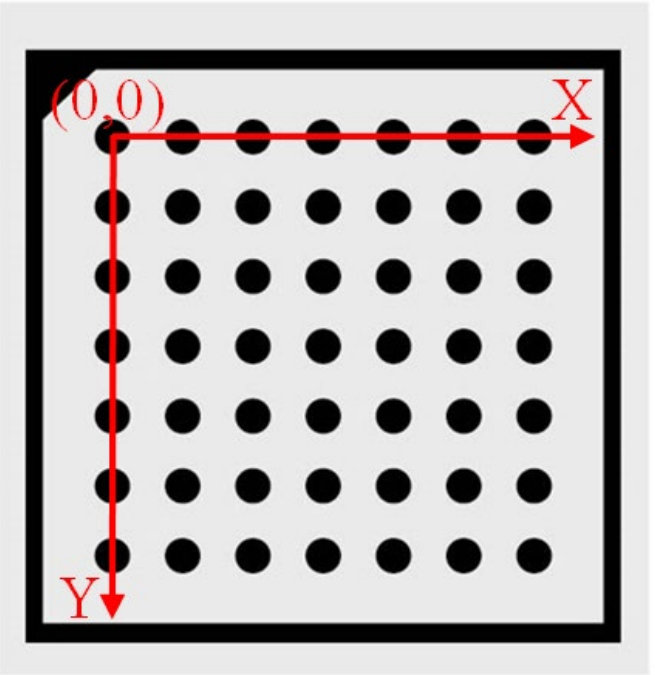

a) Halcon solid dot calibration board

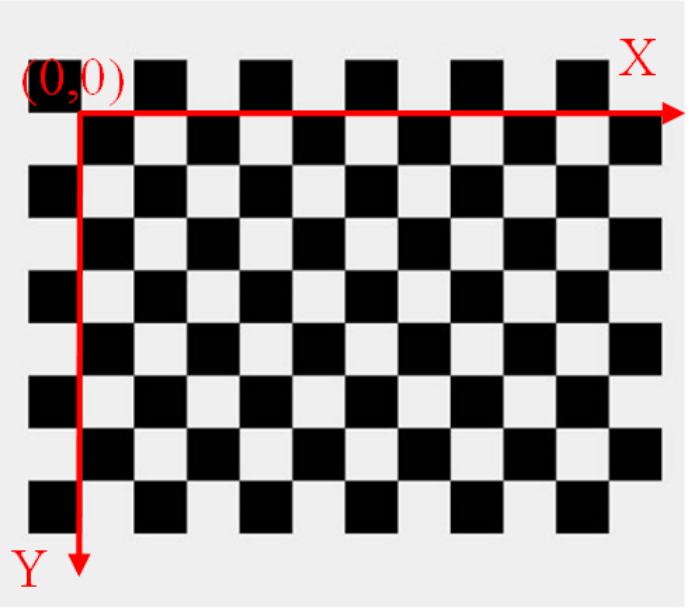

b) MATLAB checkerboard calibration boar

Fig.5. Halcon and MATLAB calibration toolbox flat calibration board

3.1. Detection and localization of calibration board feature points

3.1.1. Subpixel detection of checkerboard corner points

In this section, the Harris corner detection algorithm is used to detect checkerboard corner points, which is fast and has certain noise suppression ability. Since the accuracy of Harris corner detection is pixel level, it is necessary to use the Harris detection results as initial positions, and then within a 5×5 window of these positions, sub-pixel corner detection with high accuracy is performed again. During the experiment, two API functions (coreHarris) and (coreSubPix) provided by OpenCV were used to perform sub pixel corner detection on the chessboard using a coarse-to-fine strategy.

3.1.2. Unique coordinate positioning of checkerboard corner points

From the analysis in the previous section, it can be seen that to ensure the matching accuracy of the checkerboard corner points, it is necessary to ensure that these corner points have unique coordinate positioning on the calibration board. If the collected calibration image is incomplete, it will occur that the coordinates cannot be located. The calibration plate designed in this paper places the origin of the world coordinate system in the geometric center of the four-mark circles. Set the horizontal direction as the X-axis, the vertical direction as the Y-axis, and the Z-axis perpendicular to the checkerboard plane. The schematic diagram of the calibration board coordinate system is shown in Fig.6. According to the design size and layout structure of the chessboard grid, all corner points of the chessboard grid have unique coordinate positioning. We generally set the world coordinate of the corners of a chessboard as $M_i = (X_i, Y_i, Z_i)$, and since the Z-coordinate of all corners on the chessboard is zero, it can be simplified as $M_i = (X_i, Y_i)$, Among them, the world coordinates of the center of mark points numbered 1~4 are (-42,28), (42,28), (-14,-28), and (14,-28) respectively.

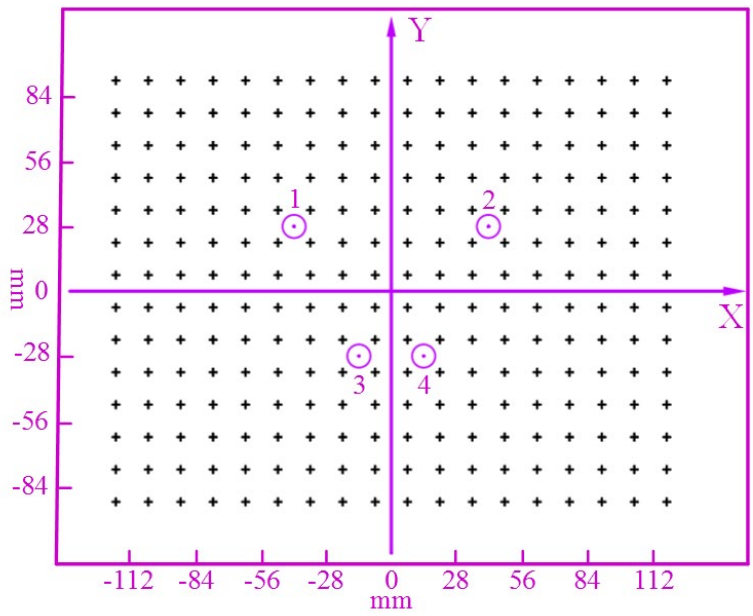

Fig. 6. Schematic diagram of the calibration board coordinate system

3.2. Guide matching of feature points on solid dot markers

3.2.1. The matching relationship between a checkerboard corner point and its imaging point on the camera

Let the world coordinate of the checkerboard corner point be $M_i = (X_i, Y_i)$, the image coordinate of its imaging point on the camera be $m_i = (u_i, v_i)$. There is a monograph mapping relationship between the checkerboard corner point coordinate M_i and the corresponding imaging point coordinate m_i:

$$s\begin{bmatrix} u_i \\ v_i \\ 1 \end{bmatrix} = H\begin{bmatrix} X_i \\ Y_i \\ 1 \end{bmatrix} \tag{12}$$

If the homography matrix $\boldsymbol{H}$ between m_i and M_i is known, the imaging point m_i can be mapped to the calibration board plane. The mapping coordinate corresponding to m_i is $\widehat{M}_i$. If the coordinate $\widehat{M}_i$ is in the neighborhood of the coordinate M_i of the checkerboard corner point, the matching correspondence between the checkerboard corner point M_i and its imaging point m_i on the camera can be found.

The homography matrix $\boldsymbol{H}$ can be obtained by four pairs of one-to-one corresponding imaging point coordinates (u, v) and world point coordinates (X, Y), that is, by calibrating the coordinates M_j of the four marked circles on the board and their corresponding imaging point coordinates m_j on the camera, $\boldsymbol{H}$ can be determined. The perspective projection of the center of a circle will experience positional displacement. After analysis, it was found that the four vertex angles of the checkerboard square where the solid dot is located are related to the projection coordinates of the center of the circle. That is, the intersection of the diagonal lines of the four-vertex angle perspective projection is the true projection m_j of the center of the circle coordinates M_j. Therefore, a more accurate homography matrix $\boldsymbol{H}$ can be calculated.

4. MULTI-DIMENSIONAL ONLINE MEASUREMENT EXPERIMENT OF TARGET IMAGE

(1) Synchronous image acquisition was carried out through external triggering of a binocular camera, and the measurement object used in the experiment was a square flange, as shown in Fig. 7.

(2) Adjust the position of the photoelectric sensor relative to the camera to ensure that the flange parts placed in any direction are within the field of vision of the binocular camera when triggering the photoelectric sensor. As shown in Fig. 8, the image pairs of flange parts acquired synchronously by the binocular camera, and the image sizes are 1280×960.

(3) Perform distortion correction and polar correction on the collected image pairs, so that the feature matching points of the left and right images are located on the same horizontal line. The corrected image pair is shown in Fig. 9, it can be seen from the two auxiliary lines in the figure that the Y-coordinate of the feature point pair has been aligned.

The Bouguet method for polar correction will crop the left and right images, the corrected image size is 1050×900, which is equivalent to the image taken by a standard binocular camera without any distortion. That is, the internal parameters of the left and right cameras are completely consistent, the distortion coefficients are all zero, and the coordinate system of the left and right cameras only translates along the X-direction, without rotation.

(4) Contour features of left and right image pairs were matched with edge points using gray correlation method based on polar threshold constraint. The sliding window size is set to 15*15 to find the best matching point pair. The threshold is set according to the approximate distance from the flange part to the camera. In this experiment, the distance between the flange plate and the camera is within the range of 500~700mm. The threshold constraint method eliminates mismatched points, and sub-pixel refinement processing is carried out on parallax data. Combining the standard binocular vision 3D measurement model, calculate the 3D coordinates corresponding to the feature points, and obtain the key contour point cloud map of the flange part, as shown in Fig. 10.

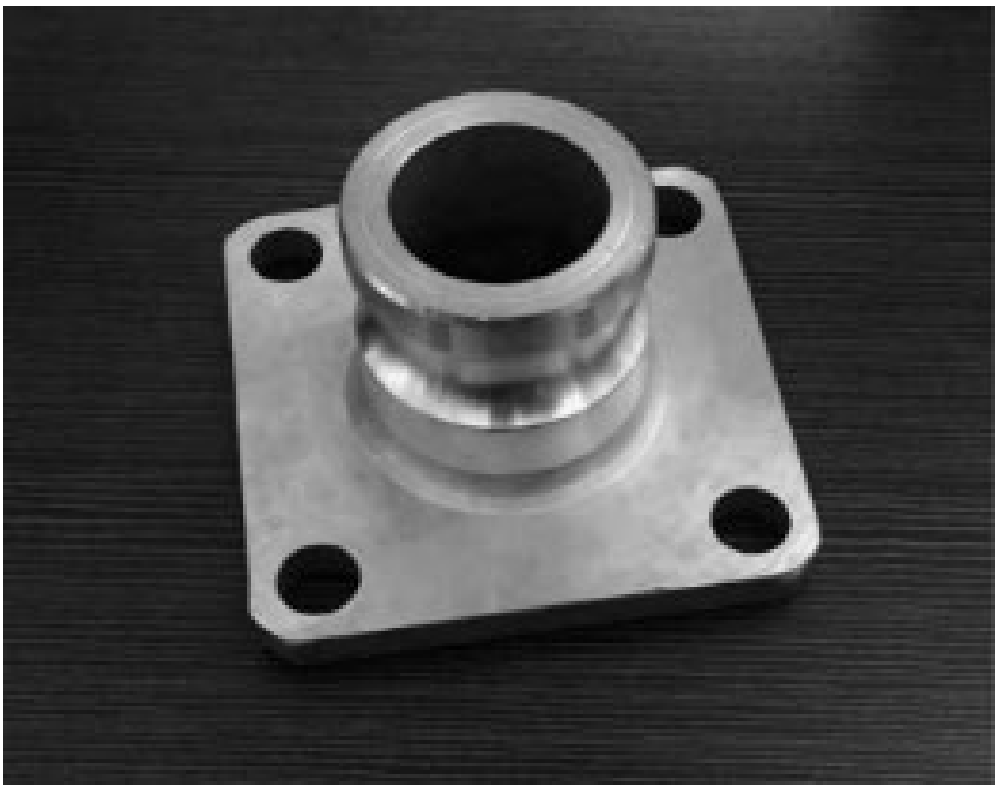

Fig. 7. Square flange parts

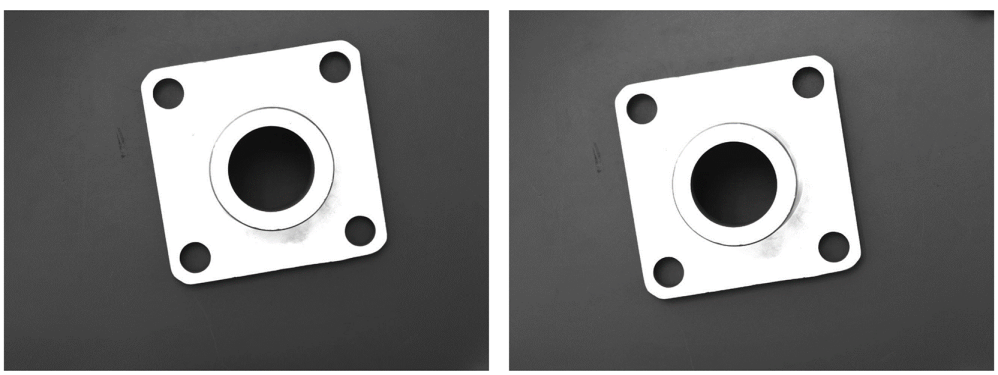

Fig. 8. Image pairs of flange parts

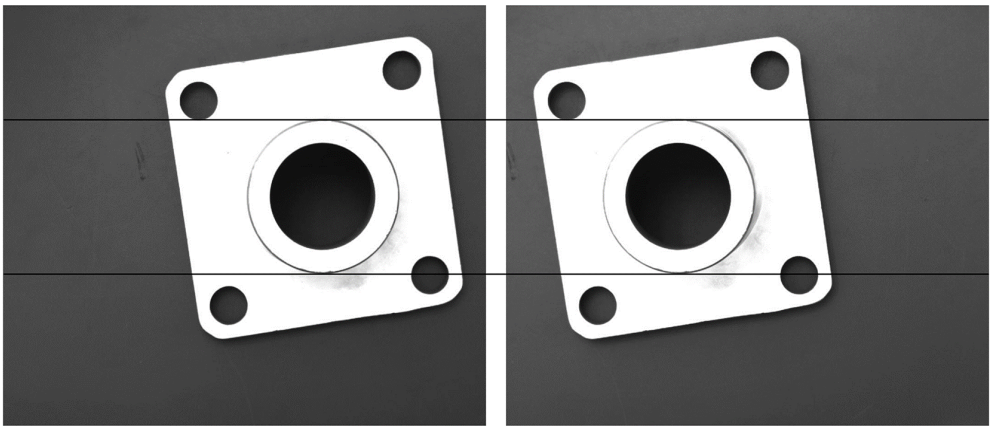

Fig. 9. Image alignment of flange parts after polar correction

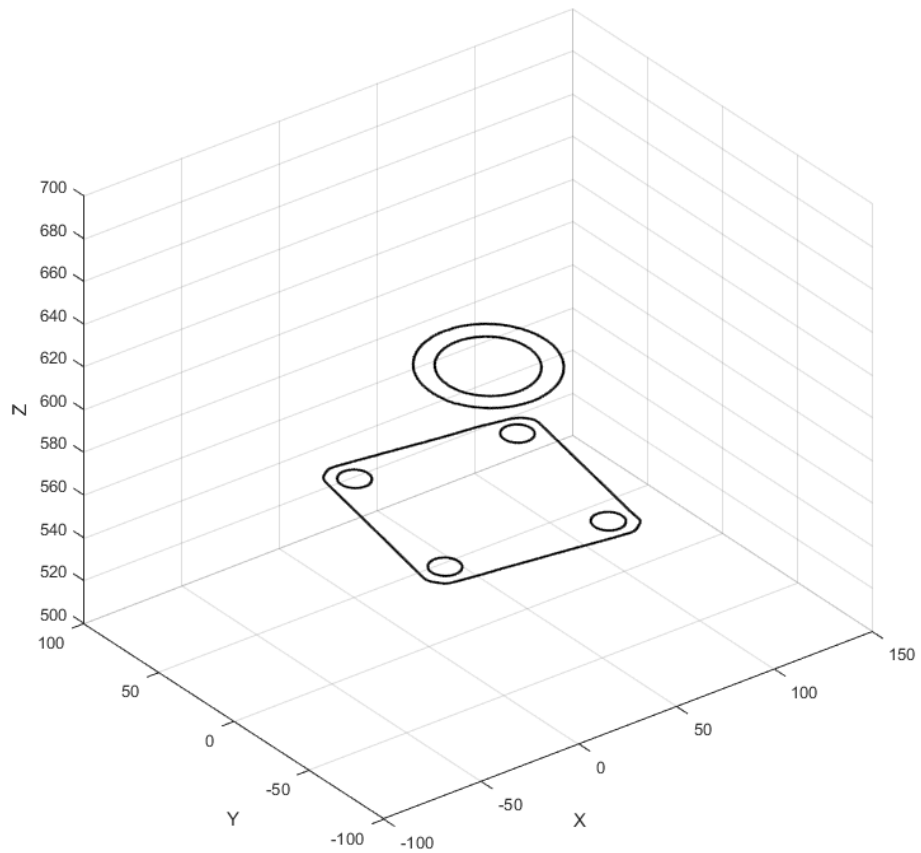

Fig. 10. Key contour point cloud diagram of flange parts

5. CONCLUSION

In this paper, in the detection of target contour features, two key points affecting the calibration accuracy of binocular camera are determined through in-depth understanding of the calibration principle of binocular camera and the study of the classic Zhang Zhengyou calibration method. The factors affecting the accuracy of these two key points are analyzed and discussed in detail. Two aspects are respectively discussed. First designing a planar calibration board based on solid dot marker guided matching, and experiments show that the calibration plate can solve the matching accuracy problem between left and right imaging points well. Second aiming at the factors affecting the calibration accuracy of monocular camera, an improved calibration method based on two-step RANSAC algorithm is proposed to improve the calibration accuracy of monocular camera. On this basis, the improved algorithm is applied to the calibration of binocular camera. The flow chart of binocular calibration based on the improved algorithm is designed, while the robustness of the method is verified by experiments.

REFERENCES

[1] Zhang, A. S., Chen, Y. P., Chen, D. W., & Tang, H., “Application of three coordinate measuring machine in reverse engineering of air compressor parts”, Mechanics and Materials Science: Proceedings of the 2016 International Conference on Mechanics and Materials Science (MMS2016), Guangzhou, China, 2017, p. 489-495.

[2] Wei, Z., & Zhang, G., “Inspecting verticality of cylindrical workpieces via multi-vision sensors based on structured light”, Optics and Lasers in Engineering, 2005, 43(10): p. 1167-1178.

[3] Jiang, L., Wu, S., Wu, D., & Eng, H., “Head modeling using color unequal phase stepping method”, 12th International Conference on Image Analysis and Processing, 2003.Proceedings., Mantova, Italy, IEEE. 2003, p. 94-98.

[4] Singh, R., Baby, B., Suri, A., & Anand, S., “Comparison of laser and structured light scanning techniques for neurosurgery applications”, 2016 3rd International Conference on Signal Processing and Integrated Networks (SPIN), Noida, India, IEEE, 2016, p. 301-305.

[5] Rubez, G., Etancelin, J. M., Vigouroux, X., Krajecki, M., Boisson, J. C., & Hénon, E., “GPU accelerated implementation of NCI calculations using promolecular density”, Journal of Computational Chemistry, 2017, 38(14): p. 1071-1083.

[6] Yu, S., Zhang, J., Yu, X., Sun, X., & Wu, H., “Unequal-period combination approach of gray code and phase-shifting for 3-D visual measurement”, Optics Communications, 2016, 374: p. 97-106.

[7] Cubero, S., Aleixos, N., Moltó, E., Gómez-Sanchis, J., & Blasco, J., “Advances in machine vision applications for automatic inspection and quality evaluation of fruits and vegetables”, Food and Bioprocess Technology, 2011, 4(4): p. 487-504.

[8] Tsai, R. Y., “An efficient and accurate camera calibration technique for 3D machine vision”, Proc. IEEE Conf. Computer Vision and Pattern Recognition, 1986, p. 364-374.

[9] Zhang, Z., “A flexible new technique for camera calibration”, IEEE Transactions on Pattern Analysis and Machine Intelligence, 2000, 22(11): p. 1330-1334.

[10] Luong, Q. T., & Faugeras, O. D., “Self-calibration of a moving camera from point correspondences and fundamental matrices”, International Journal of Computer Vision, 1997, 22(3): p. 261-289.

[11] Krüger, L., & Wöhler, C., "Accurate chequerboard corner localisation for camera calibration", Pattern Recognition Letters, 2011, 32(10): p. 1428-1435.

[12] Bennett, S., & Lasenby, J., "ChESS-Quick and robust detection of chess-board features", Computer Vision and Image Understanding, 2014, 118(1): p. 197-210.

[13] Chu, J., GuoLu, A., & Wang, L., "Chessboard corner detection under image physical coordinate", Optics and Laser Technology, 2013, 48(6): p. 599-605.

[14] Luo, P. F., & Wu, J., "Easy calibration technique for stereo vision using a circle grid", Optical Engineering, 2008, 47(3): p. 281-291.

[15] Jiang, G., & Quan, L., "Detection of concentric circles for camera calibration", Tenth IEEE International Conference on Computer Vision (ICCV'05), Beijing, China, IEEE, 2005, 1: p. 333-340.

[16] Ma, J., & Li, B., "A method of camera calibration by iterative optimization algorithm", Proceedings of the 2013 International Conference on Advanced Mechatronic Systems, Luoyang, China, IEEE, 2013, p. 302-305.

[17] Zhou, F., Cui, Y., Peng, B., & Wang, Y., "A novel optimization method of camera parameters used for vision measurement", Optics and Laser Technology, 2012, 44(6): p. 1840-1849.

[18] Ricolfe-Viala, C., & Sanchez-Salmeron, A. J., "Camera calibration under optimal conditions", Optics Express, 2011, 19(11): p. 10769-10775.

[19] Muruganantham, C., Jawahar, N., Ramamoorthy, B., & Giridhar, D., "Optimal settings for vision camera calibration", The International Journal of Advanced Manufacturing Technology, 2009, 42(7): p. 736-748.

[20] Harris, C., & Stephens, M., "A Combined corner and edge detector", Alvey Vision Conference, 1988, 15(50): p. 10-5244.

[21] Fischler, M. A., & Bolles, R. C., "Random sample consensus: a paradigm for model fitting with applications to image analysis and automated cartography", Communications of the ACM, 1981, 24(6): p. 381-395.

[22] Canny, J., "Computational approach to edge detection", IEEE Transactions on Pattern Analysis and Machine Intelligence, 1986, 8(6): p. 679-698.

[23] Lowe, D. G., "Distinctive Image features from scale-invariant keypoints", International Journal of Computer Vision, 2004, 60(2): p. 91-110.

[24] Bergholm, F., "Edge focusing", IEEE Transactions on Pattern Analysis and Machine Intelligence, 1987, 9(6): p. 726-741.

[25] He, S., Tong, Z., Ma, G., Fan, M., Lingzhou, L., & Tang, S., Research on stereo vision matching algorithm for rescue robot", 2017 International Conference on Robotics and Automation Sciences (ICRAS), Hong Kong, China, IEEE, 2017, p. 35-38.

[26] Nalpantidis, L., & Gasteratos, A., "Stereo vision for robotic applications in the presence of non-ideal lighting conditions", Image and Vision Computing, 2010, 28(6): p. 940-951.

[27] Li, Z. Y., Song, L. M., Xi, J. T., Guo, Q. H., Zhu, X. J., & Chen, M. L., "A stereo matching algorithm based on SIFT feature and homography matrix", Optoelectronics Letters, 2015, 11(5): p. 390-394.

[28] Li, C. L., Chang, Z. Y., & Mo, R., "Phase-based stereo matching by using improved LMedS algorithm and greedy strategy", Journal of Computer-Aided Design and Computer Graphics, 2014, 26(11): p. 2047-2055.

[29] Huang, X. D., Meng, T. W., Ding, D. X., & Wang, Z. H., “A novel phase difference frequency estimator based on forward and backward sub-segmenting”, Acta Physica Sinica, 2014, 63(21): p. 214304.